2020 SNMMI Highlights Lecture: General Nuclear Medicine and Molecular Imaging

Heather A. Jacene, MD, Dana-Farber Cancer Institute, Brigham and Women's Hospital, and Harvard Medical School, Boston, MA

From the Newsline Editor: The Highlights Lecture, presented at the closing session of each SNMMI Annual Meeting, was originated and presented for more than 30 years by Henry N. Wagner, Jr., MD. Beginning in 2010, the duties of summarizing selected significant presentations at the meeting were divided annually among 4 distinguished nuclear and molecular medicine subject matter experts. Each year Newsline publishes these lectures and selected images. The 2020 Highlights Lectures were delivered on July 14 as part of the SNMMI Virtual Annual Meeting. In this issue we feature the lecture by Heather A. Jacene, MD, associate professor in the Department of Radiology at the Dana-Farber Cancer Institute, Brigham and Women's Hospital, and Harvard Medical School (Boston, MA), who spoke on highlights in general nuclear and molecular imaging. Note that in the following presentation summary, numerals in brackets represent abstract numbers as published in The Journal of Nuclear Medicine *(2020;61[suppl 1]).*

It is a delight to present the General Nuclear Medicine highlights for this virtual 2020 SNMMI Annual Meeting. This year, there were 135 abstracts (79 accepted as oral presentations and 56 as posters) presented in the General Clinical Nuclear Medicine track, covering musculoskeletal (18), gastroenterology (10), renal (14), pediatric (13), infectious disease (23), and nontherapy endocrinology (57) topics in 10 oral and 6 poster sessions. Abstract submissions again came from around the world, with the United States (57) and China (23) having the highest number, followed by India (12), Japan (7), and Canada (5), with many other countries represented. I thank everyone who sent slides for this presentation and regret that time limitations prevent sharing all of the excellent work presented at this year's meeting. In this year's unusual virtual format, I missed the face-to-face encounters at oral and poster sessions and opportunities to discuss research with authors but am encouraged by the exciting and innovative work presented.

Many of the abstracts this year hit on multiple and sometimes overlapping themes, and it was challenging to group them for this summary. I decided on 2 major categories—protocol optimization and tracer development—both of which also touch on image quality and time efficiency. Abstracts focused on new software and hardware were also related to time efficiency.

Protocol Optimization

Although ^{18}F-FDG PET/CT is used today in many instances to interrogate for infection, multiple indications remain for radiolabeled leukocyte scanning. Bhargava et al. from the Zucker School of Medicine at Hofstra Northwell (Hempstead, NY), Long Island Jewish Medical Center (New Hyde Park, NY), and MicroMedicine, Inc. (Waltham, MA) reported on "Labeled leukocyte imaging: Improved leukocyte isolation with a novel automated microfluidics-based system" [541]. Microfluidic leukocyte isolation is accomplished through a series of microchannels and microstructures that fractionate blood components. This reduces the number of radiolabeled red blood cells and platelets in the final injectate and should reduce the background blood pool appearance of the images we are accustomed to seeing. In this prospective study, 19 patients had 80 cc of whole blood withdrawn. Forty cc were sent for conventional radiolabeling and 40 cc for microfluidic isolation radiolabeling with ^{111}In-oxine (8 patients) or ^{99m}Tc-exametazime (11 patients), respectively. Superior results were found for the novel microfluidic approach. There was greater purity of the isolate from the microfluidic approach. The microfluidic technique had a shorter processing time of $<$40 minutes, compared to $>$110 minutes for the conventional technique. Greater radiolabel stability was seen for both radionuclides, with no difference between the techniques for labeling efficiency or leukocyte viability. In addition to improved image quality from purer leukocyte isolates, better isolation methods may also be of benefit in patients with low white blood cell counts, where our ability to use white blood cell imaging is limited. This research team is planning the next phase of investigation, comparing imaging results using conventionally isolated vs. microfluid-isolated white blood cells in patients with suspected arthroplasty infections.

Heather A. Jacene, MD

For evaluation of chronic cholecystitis and determining gallbladder ejection fraction (GBEF), current guidelines support 60-minute sincalide-stimulated cholescintigraphy, with a GBEF $>$38% considered as normal. Vasireddi et al. from the University of Pittsburgh/University of Pittsburgh Medical Center (PA) reported on "Sincalide-stimulated cholescintigraphy: A retrospective study and proposal of a modified workflow" [421]. They hypothesized that most subjects with a normal GBEF will achieve a normal EF by 30 minutes; if true, a shorter workflow could be implemented. The retrospective study included 302 patients, with GBEFs at 20 and 30 minutes estimated manually from time–activity curves generated at the time of the examinations. About 12% of patients (36) had abnormal GBEFs ($\leq$38%) representing chronic cholecystitis. Of the 88% (266

patients) with normal GBEFs at 60 minutes, 61% (163 patients) achieved a normal GBEF (>38%) at 20 minutes, and this increased to about 88% (233 patients) at 30 minutes. These findings agreed with the authors' hypothesis. Based on these results they proposed a new workflow, performing dynamic imaging in two 30-minute sections, stopping for a normal EF (>38%) at 30 minutes, continuing if abnormal at that time point, and then combining both sections to calculate the final GBEF. This has the potential to be time saving, particularly with experienced technical staff and physicians to gauge a normal GBEF at 30 minutes. What might be extremely important in implementing this modification on a larger scale would be the real-time ability to draw a region of interest on the gallbladder in the first 10 minutes of the study and then watch it dynamically to make the most accurate decision at the 30-minute time point. This is a challenge for software development teams in the field.

Protocol Optimization: Software/Hardware

Emerging data over the past several years support the continued investigation of ways in which the use of SPECT/CT techniques can lead to improvements in presurgical lobar lung quantification. One of the continuing challenges is accurate segmentation of the lung lobes. Performed manually, this can be quite time consuming and limits consistent comparison and widespread implementation. This is a promising area for application of artificial intelligence in general nuclear medicine. Gao and colleagues from Siemens Medical Solutions (Knoxville, TN, and Hoffman Estates, IL), Siemens Healthcare GmbH (Erlangen and Forchheim, Germany), Siemens Healthineers (Princeton, NJ), and University Hospital Basel (Switzerland) reported on "Evaluation of automatic lung lobe segmentation for SPECT/CT lung V/Q image analysis" [1489]. They evaluated the performance of an automated image analysis workflow on datasets from 15 patients with abnormal anatomy or images with limited lung fissure visibility from lower-dose CT acquisitions. In Figure 1, the top row shows the steps used for data input, landmark detection from CT, and application of a deep image-to-image network for the automated workflow to generate visualization of the lung segments and then 3D SPECT quantification. The bottom row shows 2 examples in which the automated workflow was able to identify abnormal anatomy. On the left, a smaller right superior lobe was observed in a patient with an enlarged lung as the result of emphysema. On the right, segmentation around a right upper lobe lung mass clearly differentiated the tumor. For comparison to this automated workflow, 1 nuclear medicine reader also manually performed the segmentation. The physician performing the manual segmentation then assigned the manual and automated study results into 2 groups: 1 in which there was sufficient delineation of lung fissures and a second in which there was not. A second nuclear medicine physician then graded the quality of the segmentation on a scale of 1–10 (10 being the best). In group 1, the quality of the segmentation was the same for manual and automatic segmentation. For group 2, the automated method received reasonable quality scores but not as good as the manual segmentation. When the manual and automated techniques in both groups 1 and 2 were compared quantitatively using the Dice score, segmentation results were overlapping. Most important, the automated workflow completed lung lobe segmentation successfully and generated results in <30 seconds per patient. So even in those challenging cases in which a reader needs to make manual adjust-

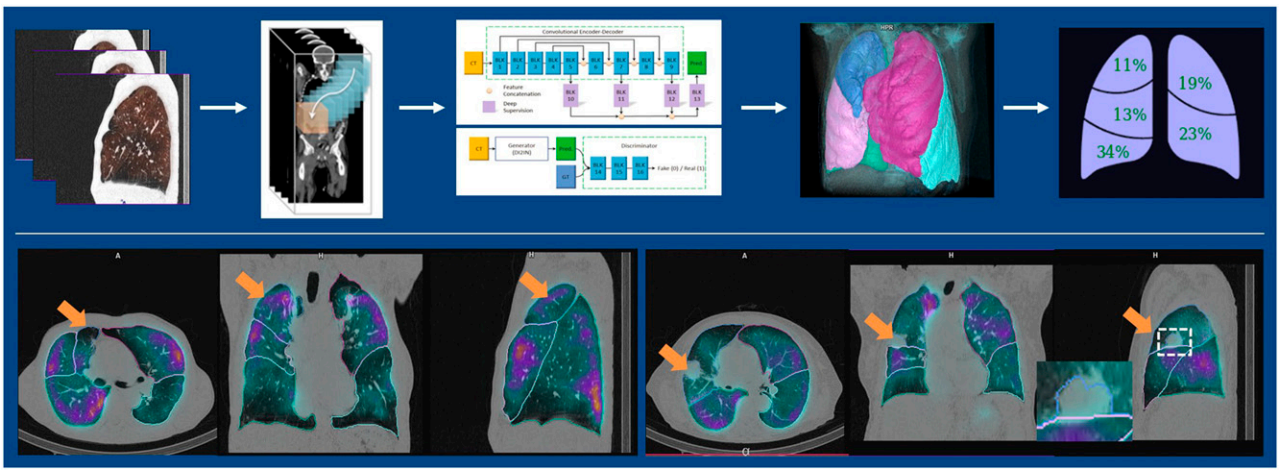

FIGURE 1. Automatic lung V/Q analysis workflow (top row, left to right): SPECT/CT volume data input, landmark detection from CT, application of a deep image-to-image network for automated workflow, resulting visualization of lung segments, and 3D SPECT quantification. Bottom: Examples of automated workflow identification of abnormal anatomy. Left block: Imaging in enlarged lung as a result of emphysema; automated workflow detected smaller right superior lobe (arrows). Right block: Segmentation around a right upper lobe lung mass clearly differentiated tumor. Automated workflow completed lung lobe segmentation successfully and generated results in <30 seconds per patient.

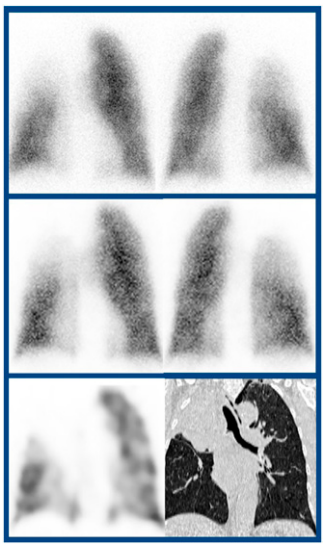

FIGURE 2. Multiview planar imaging with 360° whole-body CZT camera for presurgical assessment of lung cancer. Top block: Anterior and posterior planar images obtained with an Anger camera. Middle block: Anterior and posterior multiview planar images in the same patient. Bottom block: Coronal and low-dose CT data acquired with the multiview camera. Excellent correlation was found with conventional planar imaging for both the multiview planar and associated 3D SPECT/CT images (r^2 = 0.94 and 0.99, respectively).

ments, the time saved from such an automated workflow could be extremely valuable. Other groups are also working on similar segmentation models for lung imaging.

Several presenters at the meeting described the use of whole-body 360° cadmium-zinc-telluride (CZT) cameras and compared results with those from traditional planar imaging. Acquisition protocols with this CZT camera can be as short as 5 minutes and can generate both SPECT/CT images and reconstructed planar projections, a combination called "multiview planar" imaging. Melki et al. from the Centre Hospitalier Régional Universitaire–Nancy (Vandoeuvre-lès-Nancy, France) reported on "Assessment of multiview planar imaging provided by a high-speed 360° whole-body CZT camera in patients undergoing presurgical assessment of a lung cancer" [1488]. In this study, 20 consecutive patients undergoing presurgical assessment underwent conventional planar imaging and a CZT SPECT/CT acquisition. In an example set of images (Fig. 2), the quality and areas of abnormality in the right upper lobe of the lung appear similar between the planar and multiview planar images. One might argue that the resolution is slightly better in the multiview planar images than in those obtained with the Anger camera. Additional information is available from the SPECT/CT slices. Excellent correlation for differential lung function was seen between conventional planar and CZT SPECT/CT images (r^2 = 0.99 for 3D SPECT/CT and r^2 = 0.94 for multiview planar).

Bahloul et al., also from the Centre Hospitalier Régional Universitaire–Nancy, reported on "Dimercaptosuccinic acid (DMSA) renal investigations performed with a 360° whole-body CZT SPECT camera as compared with the conventional method based on planar images from an Anger camera" [244]. In this study, 21 consecutive patients (age range. 6 months–85 years) underwent ^{99m}Tc-DMSA scanning with a conventional Anger camera and the CZT camera. The CZT camera acquisition time was about 5 minutes. The count rate detected by the CZT camera was 180% of that with the conventional camera. Interpretations were concordant in 90% of paired image sets from the 2 cameras. The 2 discordant cases are shown in Figure 3 and were ultimately considered as having a more accurate diagnosis from the CZT camera. In the top images, a small defect not called on the planar images was visible with the CZT SPECT camera. In the bottom images, a small defect was called as a false-positive on the planar image but was shown to have contiguous cortical uptake of tracer with the CZT SPECT camera. Excellent correlation was also seen between relative kidney function with both acquisitions (r^2 = 0.98). The CZT SPECT camera technology has multiple potential advantages, including shorter acquisition times to enhance workflow, additional benefits of shorter acquisition time in reducing patient motion and improving image quality, the ability to have both SPECT/CT and planar reconstructions in a single acquisition, and the potential for reduced administered activity because of higher count rate detection.

Protocol Optimization: Bowel Transit

One theme of reports presented this year pertaining to protocol optimization related to bowel transit studies; a topic that is rarely covered in these highlights sessions. I did a quick survey of colleagues from around the country, in both academia and private practice, in preparation for this talk. Their average number of gastric emptying studies per week varied between 10 and 20, so work relating to optimization and understanding of these protocols remains relevant in general nuclear medicine practice.

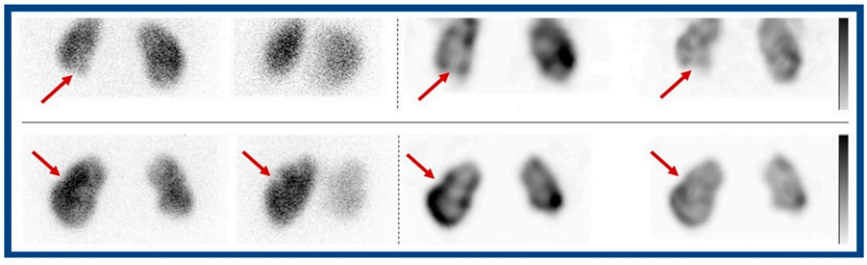

FIGURE 3. ^{99m}Tc-DMSA multiplanar view renal imaging with a whole-body CZT camera (right pairs in each set of images) vs. conventional Anger camera planar imaging (left pairs in each set of images). Although 90% of interpretations with these 2 methods were concordant in this study, these 2 were discordant. In patient 1 (top row), conventional imaging was found to be false-negative, whereas the CZT SPECT was true-positive, identifying a small cortical defect in the right inferior kidney. In patient 2 (bottom row), conventional imaging called a small defect as positive, whereas CZT SPECT correctly showed contiguous cortical uptake of the tracer. CZT camera acquisition time was about 5 minutes, with a count rate detection 180% of that with the conventional camera.

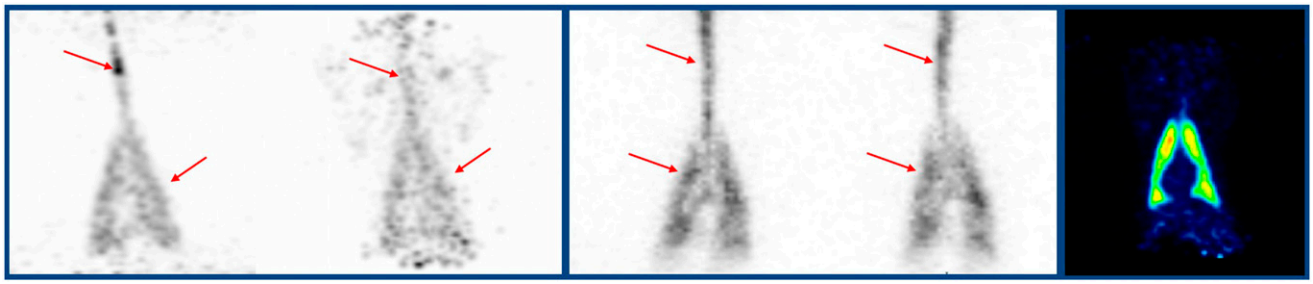

FIGURE 4. Radioaerosolized ^{18}F-fluoride-alumina nanoparticle imaging of mucociliary transport and clearance in a ferret model of cystic fibrosis. Images show ^{18}F-fluoride-alumina nanoparticle (left) and ^{99m}Tc-sulfur colloid (middle) clearance at trachea and upper/lower lobes of lung at 5 and 60 minutes after administration. Right: Early dynamic PET/CT at 5 minutes showed ^{18}F-fluoride-alumina nanoparticle activity deposition in lungs. The ultimate goal of this research is to translate the imaging technique to patients with cystic fibrosis, particularly for monitoring response to therapy.

Although gastric emptying studies are routinely performed in pediatric patients, no normal values exist for this population. At the same time, studies have shown that up to 70% of children may not be able to tolerate the complete standard meal or may require an alternate meal. Ng et al. from the Brigham and Women's Hospital, Brandeis University, and Boston Children's Hospital (all in Boston, MA) asked "How much do we need to eat? Assessment of partial standard and alternative meals for use in pediatric gastric emptying studies" [117]. In a second report, they described "Assessment of nonstandard cheese-based meals as viable alternatives to the standard adult meal for pediatric gastric emptying scintigraphy" [1580]. They performed a retrospective review of >1,000 studies to assess the applicability of the adult standard meal criterion of <10% meal retention by 4 hours after meal ingestion for partially consumed adult standard meals in the pediatric population. They also looked at the extension of this criterion to nonstandard cheese-based meals. In the cohort, 18% of the children ate partial meals and 7% ate an alternative cheese-based meal. Adult criteria were used to initially characterize the studies as normal or abnormal emptying. The authors showed data indicating no differences in classifying normal or abnormal gastric emptying comparing complete, partial, and alternate meal types across sexes and age groups. It is unethical and/or challenging to recruit normal pediatric subjects for such studies, so the authors used a data-driven clustering approach to independently verify the appropriateness of the adult criteria threshold. They showed good concordance between both methods of stratifying subjects with normal and delayed gastric emptying, further supporting the use of the adult criteria for pediatric use. They concluded that the adult criterion for normal gastric motility can be applied to children who ingest as little as 50% of the standard adult meal and that cheese-based meals offer viable alternatives to the full adult standard meal in the pediatric population. These data provide previously unavailable guidance for managing children who eat less than the full meal or an alternative meal (additionally useful as alternative meals become more common even in the adult population).

Maurer and colleagues from Temple University Hospital/Temple University School of Medicine (Philadelphia, PA) investigated the "Added value of small bowel transit scintigraphy for assessment of patients with symptoms of gastroparesis" [428]. The rationale for the research was that dyspeptic symptoms may be nonspecific and are often not correlated with the results of gastric emptying studies. The authors aimed to determine the prevalence of delayed small bowel transit in patients undergoing gastric emptying scintigraphy for symptoms of gastroparesis and to determine

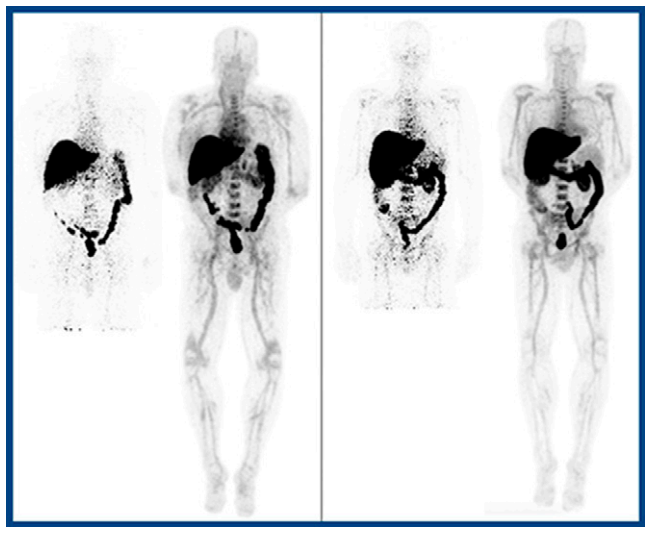

FIGURE 5. First-in-human total-body PET imaging of HIV with ^{89}Zr-VRC01 on the EXPLORER. Left: ^{89}Zr-VRC01 imaging with conventional PET (left) and the EXPLORER (right) in an antiretroviral therapy–suppressed patient (acquired at 72 hours after tracer injection). Right: ^{89}Zr-VRC01 imaging with conventional PET (left) and the EXPLORER (right) in a patient with low-level viremia. The difference in image quality between the 20-minute 1-bed position with the EXPLORER and the 30-minute 6-bed positions with a standard PET camera is clear.

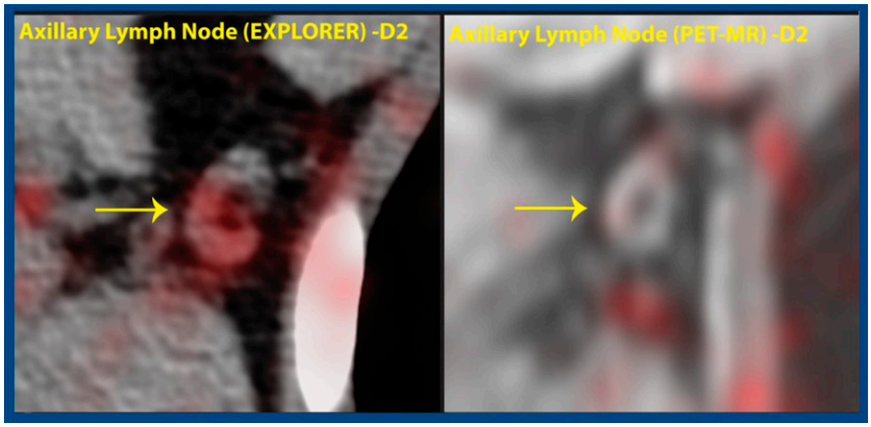

FIGURE 6. Total-body PET imaging of HIV with ^{89}Zr-VRC01 on the EXPLORER (left) showed increased axillary lymph node (arrows) 2 days after tracer injection compared with conventional PET/MR imaging (right). Increased soft tissue/blood ratios were also seen in patients with active viremia compared with those in patients with antiretroviral therapy suppression.

what symptoms are associated with delayed small bowel transit and the ways in which these differ from those associated with delayed gastric emptying. The investigation included 363 patients with evaluable studies who had undergone both a gastric emptying study and a small bowel transit study. Of these, 174 (47.9%) had delayed solid gastric emptying (>60% retention at 2 hours or >10% at 4 hours), 141 (38.8%) had delayed liquid gastric emptying (>50% retention at 1 hour), and 70 (19.3%) had delayed small bowel transit (<40% ^{111}In liquid activity reaching the terminal ileum or cecum/colon at 6 hours). Among those with delayed small bowel transit, 24 (6.6%) had isolated small bowel transit abnormalities and normal gastric emptying. Symptoms more commonly associated with isolated small bowel transit included postprandial fullness, stomach fullness, bloating, and visibly larger stomach, whereas those associated with delayed solid gastric emptying included more nausea and vomiting. The authors concluded that the addition of small bowel transit studies to gastric emptying scintigraphy may explain some of the symptoms of patients presenting with upper gastrointestinal dyspepsia and/or suspected gastroparesis. Many clinical sites do not perform small bowel transit studies because of the amount of time required, but these preliminary data suggest the potential for tailoring studies based on individual patient symptoms.

Development: New Tracers

Last year at the SNMMI Annual Meeting, a group of researchers presented their initial work on a novel radiotracer, ^{18}F-fluoride-alumina nanoparticles, to visualize mucociliary transport and clearance in a pig model, but translatability was limited as the agent had to be administered via an endotracheal tube. This year, the same team continued their work with the development of a radioaerosolized version of the nanoparticles. Akurathi et al. from the University of Iowa/University of Iowa Carver College of Medicine (Iowa City) reported on "Evaluation of lung mucociliary transport and clearance in ferrets: Imaging nebulized radioaerosols" [1490]. Their cystic fibrosis ferret model reflects the full spectrum of cystic fibrosis phenotypes observed in human patients. The ^{18}F-fluoride alumina nanoparticles (particle size ≤50 nm) had good clearance from the trachea during the initial phase of dosing (<5 minutes), faster than was seen

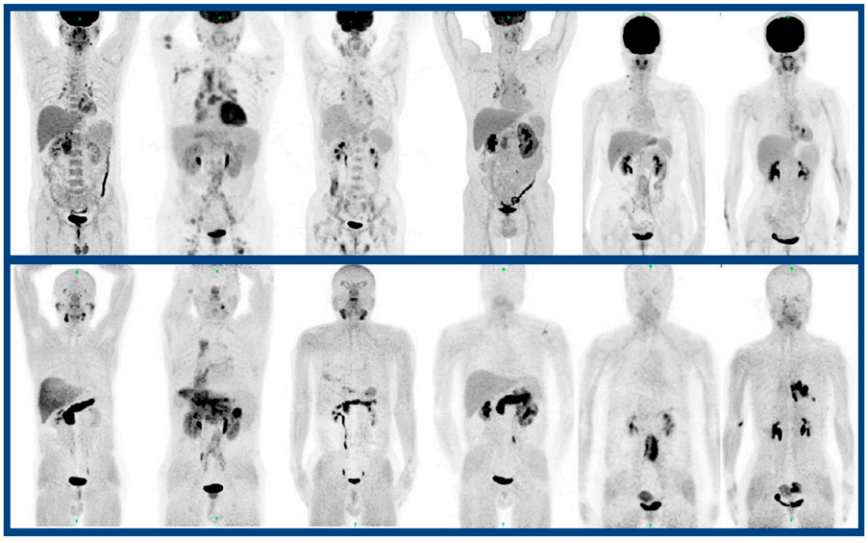

FIGURE 7. "^{68}Ga-FAPI PET/CT imaging of fibrosis in IgG4-related disease. Top row: ^{18}F-FDG PET/CT imaging in a series of 5 patients with IgG4-related disease. Bottom row: Corresponding ^{68}Ga-FAPI PET/CT images acquired in the same patients. ^{68}Ga-FAPI PET/CT showed a larger number of organs involved in about half of patients, with the most involvement identified in the pancreas, salivary glands, bile duct/liver, and lacrimal glands. ^{18}F-FDG uptake was higher in the lymph nodes, but this is associated with less morbidity. This work highlighted the ways in which different tracers can show varying aspects of disease, in this case organ vs. nodal involvement.

for the comparative ^{99m}Tc-sulfur colloid agent (particle size, 0.03–10 μm) (Fig. 4). The time–activity curve showed the rapid clearance of the ^{18}F-labeled nanoparticle. Given the imaging properties of ^{18}F and the ability to perform early dynamic PET/CT scanning, ^{18}F-fluoride-alumina nanoparticles have the potential for expanded studies in small animal cystic fibrosis models. The team's ultimate goal is to translate this imaging technique to patients with cystic fibrosis, particularly for monitoring response to therapy.

Exciting technology and tracers previously presented in oncology are making their way into general nuclear medicine applications. Beckford-Vera and colleagues from the University of California at San Francisco, the University of California at Davis, and the University of California Davis Medical Center (Sacramento) presented "First-in-human total-body PET imaging of HIV with ^{89}Zr-VRC01 on the EXPLORER" [545]. HIV can persist in anatomic reservoirs and rebound if successful antiretroviral therapy is stopped. The ability to assess this viral burden, however, remains a challenge. VRC01 is a broadly neutralizing monoclonal antibody that binds HIV envelope glycoprotein 120. Figure 5 compares images acquired with conventional PET/MR to images acquired with the EXPLORER, the first total-body PET/CT device. The image on the left is of an antiretroviral therapy–suppressed patient, and on the right is a patient with low-level viremia. The difference in image quality between the 20-minute 1-bed position with the EXPLORER and the 30-minute 6-bed positions with a standard PET camera is clear. Figure 6 shows increased sensitivity for detection of antibody uptake in a small node with the EXPLORER. Increased soft tissue/blood ratios were also seen in patients with active viremia compared with those in patients with antiretroviral therapy suppression. The authors concluded that "utilization of total-body imaging demonstrates the potential to inform on whole-body anatomical localization and burden of persistent HIV infection." The abilities of the total-body PET EXPLORER open up possibilities for the use of many tracers, such as antibody imaging, that have typically been more challenging in the past.

Luo et al. from Peking Union Medical College Hospital (Beijing, China) investigated "^{68}Ga-FAPI PET/CT for imaging of fibrosis in IgG4-related disease: Comparison to ^{18}F-FDG PET/CT" [544]. IgG4-related disease causes significant morbidity and mortality, primarily as the result of organ dysfunction from uncontrolled and progressing fibrosis. The diagnosis is based on serum IgG4 blood plasmablast concentration ratios, but these do not localize disease in a way that can guide tissue biopsy. The team studied 26 patients with both ^{18}F-FDG and ^{68}Ga-FAPI. ^{68}Ga-FAPI PET/CT showed a larger number of organs involved in about half of patients, with the most involvement identified in the pancreas, salivary glands, bile duct/liver, and lacrimal glands (Fig. 7). Of note, ^{68}Ga-FAPI uptake was higher in the pancreas and liver, organs in which progressing fibrosis could result in significant organ dysfunction and morbidity. ^{18}F-FDG uptake was higher in the lymph nodes, but this is associated with less morbidity.

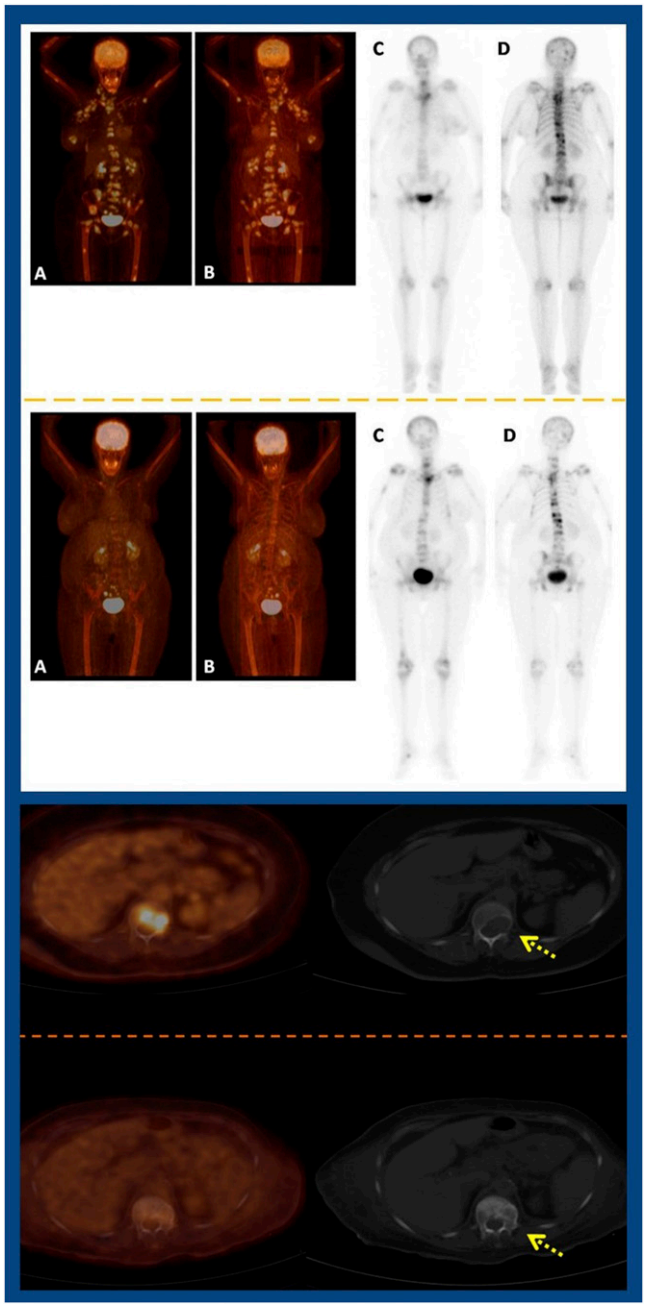

FIGURE 8. ^{18}F-FDG PET/CT and ^{99m}Tc-MDP bone scintigraphy in estimation of metastatic osseous burden in breast cancer patients. A semiquantitative metastatic osseous score based on PET was more closely correlated with changes in tumor and bone markers than bone scan score. Top, left block, top and bottom: ^{18}F-FDG PET/CT imaging in 2 patients before and after treatment. Middle block: Comparative ^{99m}Tc-MDP bone scintigraphy before and after treatment in the same patients. PET scores decreased but the bone scan scores remained the same. Bottom block: Example of an ^{18}F-FDG-avid lytic lesion that became non-FDG avid after treatment and was sclerotic on follow-up.

The authors concluded that ^{68}Ga-FAPI might be a promising imaging agent for assessment of IgG4-related disease. This work highlighted the ways in which different tracers can show

varying aspects of disease (in this case, organ vs. nodal involvement). Future studies investigating these agents must work to align clinical questions with clinically relevant endpoints.

I will end this summary with a disease setting seen every day in the nuclear medicine clinic: breast cancer bone metastases, where the question of bone scanning vs. ^{18}F-FDG PET is a growing focus. Nasr and colleagues from Cairo University Hospital (Egypt), Prince Sultan Military Medical City (Riyadh, Saudi Arabia), and Assuit University Hospital (Egypt) reported on the "Difference between ^{18}F-FDG PET/CT and ^{99m}Tc-methyl diphosphonate (^{99m}Tc-MDP) bone scintigraphy in estimation of metastatic osseous burden in breast cancer patients: A comparative study in view of CA15-3 and alkaline phosphatase" [609]. In 37 patients with breast cancer metastasized to bone, they showed (not surprisingly) that a semiquantitative metastatic osseous score based on ^{18}F-FDG PET was more closely correlated with changes in tumor and bone markers than a bone scan score. Comparative examples in Figure 8 show ^{18}F-FDG uptake throughout the bones. Although uptake is evident in the ^{99m}Tc-MDP bone scan, it does not have the same extent or detail as the PET/CT. After successful treatment in this study, PET scores decreased but the bone scan scores remained the same. Figure 8 also shows a classic example of an FDG-avid lytic lesion that became non-FDG-avid and sclerotic after treatment. The bone scan remains the go-to test in many clinics and clinical trials assessing response in metastatic breast cancer, but here we see an example of old bread-and-butter imaging concepts that we may not be optimizing to their fullest potential.

Conclusion

This is an exciting time in general nuclear medicine, with new and potentially transforming technologies and methods. We have seen here only a few examples of the outstanding work presented at this meeting. Going forward, we must be engaged and work closely with our clinical colleagues to demonstrate benefits in workflow and/or outcomes. I am optimistic that if we do this as a community, we can continue to advance general nuclear medicine.

COVID-19 and Ventilation/Perfusion (V/Q) Lung Studies

On August 28 SNMMI released updates to a previous statement responding to concerns regarding ventilation/perfusion (V/Q) lung scans and, specifically, the inherent risk of spread of COVID-19 to patients and staff from the ventilation portion of this study. At the time of the release of the original statement on March 19, many institutions opted not to perform ventilation studies. In the interim, the COVID-19 pandemic has evolved in different ways depending on institutions, locations, and populations, with questions about the timing and safety of resuming performance of the ventilation portion of V/Q studies.

The transmissibility of COVID-19 associated with medical ventilation systems has not yet been fully elucidated. In some situations, it may remain appropriate not to perform ventilation studies, for example, in institutions or practices in areas of high or increasing COVID-19 prevalence or where access to COVID-19 testing is inadequate.

The goal of the updated statement was to recognize that, in some regions and clinical situations, a ventilation study may be deemed to be clinically necessary to help diagnose lung disease, including vascular and airway disease. In these settings, performance of ventilation studies may be considered, with local and institutional COVID-19 policies and procedures for aerosol-generating and nonaerosolizing procedures serving as the primary source of guidance. The following considerations, which typically are included in facility policies and procedures, should be reviewed prior to performing ventilation studies:

1. In general, patients should have documentation of a negative COVID-19 polymerase chain reaction test; however, in some cases, local policies or regulations may be different.
2. Technologists should wear appropriate personal protective equipment (PPE) when performing ventilation studies, consistent with local policies for the performance of aerosol-generating and nonaerosolizing procedures.
3. Airflow in the room in which ventilation studies are performed should be evaluated, which may help determine the required time for room turnover after such studies.
4. The availability and administration feasibility of ventilation agents—including FDA-approved agents such as ^{99m}Tc-DTPA, ^{133}Xe gas, and other agents (e.g., ^{99m}Tc-labeled fine carbon particles or ^{99m}Tc-sulfur colloid)—should be considered for performance of ventilation studies.
5. It is recommended that local infection control groups be engaged for guidance and to help evaluate facilities, equipment, and staff PPE use for performing ventilation studies.
6. The approach to performing a ventilation scan in relation to the perfusion scan (i.e., ventilation then perfusion vs. perfusion then ventilation) should be considered on a case-by-case basis, depending on the clinical indication and in consultation with the referring physician.

SNMMI will continue to monitor the COVID-19 pandemic and provide updated information whenever possible.

SNMMI

SNMMI Launches Updated Learning Center and Webinars Hub

Virginia Pappas, CAE, SNMMI CEO

It is difficult to believe that we are now 6 months into the COVID pandemic. Many of us have settled into a new normal: nuclear medicine departments are returning to routine operations, the school year has begun, and the new year will soon be upon us. With the ever-changing nature of COVID-19 and the pandemic landscape, it is more important than ever to update our knowledge in order to be ready for whatever the new year brings.

Education is a critical part of SNMMI's mission, and, in this time of many challenges, flexibility is key. As your professional society, SNMMI has been working tirelessly to offer high-quality content that meets your needs in a format that is easily accessible, engaging, and can fit it into your schedule, whether you are in the clinic or working remotely—in the United States or anywhere around the globe.

New Learning Center. SNMMI recently redesigned and upgraded its Learning Center with a clean new look and an improved, intuitive feel that allows easy access to the society's thriving virtual curriculum. The new center allows you to easily view all courses or limit the display to those available for the specific type of continuing education credit you need, sorting by release date or title. If you prefer, you can search all courses by keyword using the search field at the top of the screen. If you have activities already in progress, you can reach them with a single click via the top navigation. One more click brings you to your updated transcript or to the Joint Provider Portal. You can access the new Learning Center on the SNMMI website by clicking on "Education" on the top navigation bar or going to www.snmmi.org/education.

New Webinars Hub. SNMMI continues to offer an active and well-attended program of webinars, most of which are free to members. The society's new Webinars Hub puts all the information you need at your fingertips, including not only upcoming webinars but also more than 50 recorded webinars that are available on demand, many with continuing education and SAM credit. For a full list of upcoming webinars and recordings, visit the Hub at www.snmmi.org/webinars.

Mid-Winter Meeting. New educational opportunities will be available at the SNMMI Mid-Winter Meeting and American College of Nuclear Medicine (ACNM) Annual Meeting, which will take place January 28–30. This year's themed track will spotlight radionuclide therapy, from patient care coordination and safety considerations to treatment options and emerging technologies. The general nuclear medicine track will include sessions designed to expand knowledge on the latest clinical applications and best practices in the field advancing precision medicine, led by experts from SNMMI's specialty councils and centers of excellence. The ACNM 2021 Annual Meeting track will feature a robust program of cutting-edge educational content and oral presentations.

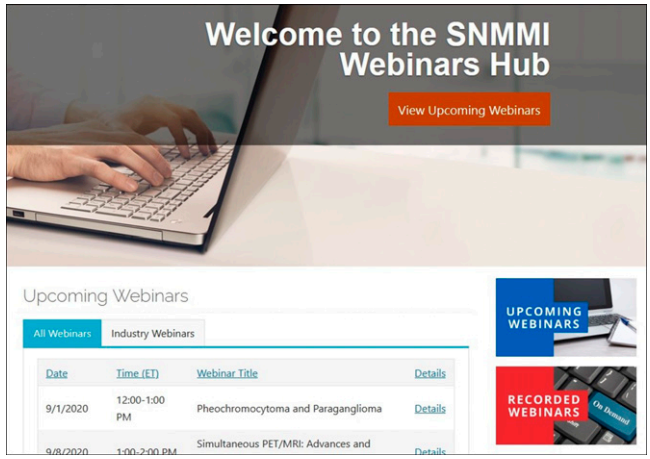

Abstracts for the meeting are welcome and can be submitted through Monday, November 2, on the following tracks:

- Radionuclide Therapy
- Aspects of Clinical and Basic Science in Nuclear Medicine
- Correlative Imaging in Nuclear Medicine and Radiology
- Nuclear Pharmacy and Physics
- Nuclear Cardiology
- Quality and Safety in Nuclear Medicine

More information on the meeting will be serially available at www.snmmi.org/MWM.

Virtual Annual Meeting. Content from SNMMI's 2020 Virtual Annual Meeting, held in June, is still available and free to all members. All content—much of it with continuing education credit—is available for a full year (through June 2021) via the virtual platform. Sessions that were offered live can be accessed on demand via the "Live Session Auditorium"; all scientific abstract and poster presentations are available via the Science Pavilion; and exhibits are still accessible in the Exhibit Hall.

Now, more than ever, education is essential for career growth and maintaining a healthy, vigorous profession. Please know that SNMMI is here to support you in any way we can. We encourage you to connect with us with any issues or questions. For a full list of contacts, visit www.snmmi.org/contact.

Each month the editor of Newsline selects articles on diagnostic, therapeutic, research, and practice issues from a range of international publications. Most selections come from outside the standard canon of nuclear medicine and radiology journals. These briefs are offered as a monthly window on the broad arena of medical and scientific endeavor in which nuclear medicine now plays an essential role. The lines between diagnosis and therapy are sometimes blurred, as radiolabels are increasingly used as adjuncts to therapy and/or as active agents in therapeutic regimens, and these shifting lines are reflected in the briefs presented here. We have also added a small section on noteworthy reviews of the literature.

Short-Term Memory and Tau and Amyloid Burden Assessment

In an article e-published on August 21 ahead of print in *Alzheimer's Research and Therapy*, Norton et al. from Massachusetts General Hospital/Harvard Medical School (Boston, MA), Gordon College (Wenham, MA), the University of Strathclyde (Glasgow, UK), the Autonomous University of the Caribbean (Barranquilla, Colombia), Brigham and Women's Hospital (Boston, MA), Universidad de Antioquia (Medellin, Colombia), and the Banner Alzheimer's Institute (Phoenix, AZ) reported on a comparison of Visual Short-Term Memory (VSTM) binding tests with direct in vivo PET measurements of amyloid and tau levels with ^{11}C-Pittsburgh compound B and ^{18}F-flortaucipir, respectively. This comparison of behavioral and neurochemical markers was conducted in individuals with the presenilin-1 E280A mutation predisposing to Alzheimer disease (AD), including 21 clinically unimpaired subjects and 7 with early mild cognitive impairment, as well as 30 family members without the mutation. The authors found that VSTM performance correlated strongly with tau PET findings in the entorhinal cortex and inferior temporal lobe and, in asymptomatic carriers, with amyloid burden. They identified interesting questions raised by the relationship between PET data results and aspects of the VTSM test in early AD and concluded that "it will be necessary to continue exploring the precise stimulus conditions that are optimal for serving as a proxy for biochemical pathology in AD or for discriminating between individuals with and without preclinical AD."

Alzheimer's Research and Therapy

Chemotherapy, Liver Injuries, and SPECT

Truant et al. from the University of Lille/CHRU Lille, INSERM Lille, and Biopredic Laboratory (Rennes; all in France) reported on August 24 ahead of print in the *Annals of Surgical Oncology* on a study designed to assess the ability of ^{99m}Tc-mebrofenin SPECT hepatobiliary scintigraphy to predict the likelihood of liver dysfunction from chemotherapy and/or chemotherapeutic-associated liver injuries, such as sinusoidal obstruction syndrome and nonalcoholic steatohepatitis. The study included 115 patients scheduled for major hepatectomy (defined as ≥3 segments) who underwent presurgical SPECT hepatobiliary scintigraphy to measure segmental liver function. Imaging results were compared between patients with and without (1) preoperative chemotherapy and (2) chemotherapy-associated liver injuries. Other factors were included in the analysis. A total of 55 (47.8%) patients received chemotherapy, 16 of whom developed sinusoidal obstruction syndrome and 35 experienced nonalcoholic steatohepatitis, with worse postoperative outcomes. However, chemotherapy had no impact on liver function, except when >12 cycles were administered. In patients with chemotherapeutic-associated liver injuries, steatosis ≥30% significantly compromised function, as did nonalcoholic steatohepatitis. Other factors impairing function were diabetes, overweight/obesity, and fibrosis. The authors concluded that ^{99m}Tc-mebrofenin SPECT hepatobiliary scintigraphy appeared to be "a valuable tool to select heavily treated patients at risk of liver dysfunction through steatosis or nonalcoholic steatohepatitis."

Annals of Surgical Oncology

^{68}Ga-PMSA PET Before Radical Prostatectomy

In an article e-published on August 21 ahead of print in *Prostate Cancer and Prostatic Diseases,* Koseoglu et al. from the Koç University School of Medicine/Koç University Hospital and the VKF American Hospital (both in Istanbul, Turkey) reported on a study investigating the incremental contribution of ^{68}Ga–prostate-specific membrane antigen (^{68}Ga-PMSA) PET as a primary staging tool in patients with prostate cancer in single Prostate Imaging Reporting & Data System (PI-RADS) 4 or 5 index lesions. The study included 81 biopsy-naïve patients (49 with PI-RADS 4 and 32 with PI-RADS 5 index lesions) who underwent multiparametric MR and ^{68}Ga-PMSA PET imaging before radical prostatectomy. Characteristics of dominant and nondominant tumors as assessed postoperatively were compared with index lesion imaging findings. ^{68}Ga-PMSA PET identified dominant tumors in 100% of patients, including 13 in whom MR was negative. ^{68}Ga-PMSA PET accurately identified nondominant tumors in 24 of 45 (53.3%) patients. Six patients (12.2%) in the PI-RADS 4 group were upgraded; ^{68}Ga-PMSA PET localized the dominant tumor in each of these patients, and MR missed the location in 2. Eight patients (25%) in the PI-RADS 5 group were upgraded; both imaging modalities accurately located the dominant tumor in each of these patients. Detection rates for extracapsular extension and seminal vesicle invasion were 51.1% and 53.8%, respectively, with MR imaging and 27.9% and 30.7%, respectively, with PET. When the 2 modalities were combined, detection rates for extracapsular extension and seminal vesicle invasion

increased to 65.1% and 61.5%, respectively. In addition, ^{68}Ga-PMSA PET identified 6 of 10 patients with positive lymph nodes, whereas multiparametric MR imaging identified none. The authors concluded that ^{68}Ga-PMSA PET has a better diagnostic accuracy in detecting dominant and nondominant tumors, in upgrading, and in adverse pathology in patients with PI-RADS 4 index lesions and that multiparametric MR imaging has a different set of predictive advantages in this setting.

Prostate Cancer and Prostatic Diseases

PET/CT and Smoldering Multiple Myeloma

Zhou et al. from the University Hospital of Würzburg and the University of Augsburg (both in Germany) reported on August 18 ahead of print in *Cancers (Basel)* (2020;12[8]:E2333) on a study exploring correlations between imaging patterns and clinical features in patients with smoldering multiple myeloma who underwent simultaneous PET/CT imaging with ^{18}F-FDG, ^{11}C-methionine, and ^{68}Ga-pentixafor. The study included 10 patients who also underwent bone marrow biopsy at the time of imaging. The authors found a significant correlation between bone marrow plasma cell infiltration and SUV_{mean} for lumbar vertebrae L2–L4 on ^{11}C-methionine PET/CT and ^{68}Ga-pentixafor PET/CT but no significant correlation between bone marrow involvement in these lumbar vertebrae and ^{18}F-FDG uptake. Mean target-to-background ratios for these lumbar vertebrae on ^{11}C-methionine PET/CT and ^{68}Ga-pentixafor PET/CT also correlated with bone marrow plasma cell infiltration, with no similar correlation with ^{18}F-FDG uptake. ^{11}C-methionine PET/CT also showed a significant correlation between bone marrow plasma cell infiltration and maximum target-to-background ratios in the target lumbar vertebrae. The authors summarized their findings that "^{11}C-methionine and ^{68}Ga-pentixafor PET/CT demonstrate higher sensitivity than ^{18}F-FDG PET/CT in detecting bone marrow involvement in smoldering multiple myeloma."

Cancers (Basel)

^{225}Ac-PSMA-617 Targeted Therapy in MCRPC

In a study published on July 23 in *Theranostics* (2020;10[20]:9364–9377) Yadav et al. from the All India Institute of Medical Sciences (New Delhi) reported on the safety and therapeutic efficacy of ^{225}Ac–prostate-specific membrane antigen-617 (^{225}Ac-PSMA-617) targeted α therapy in metastatic castration-resistant prostate cancer. The study included 28 men (mean age, 69.7 y; range, 46–87 y), 15 of whom who were refractory to previous ^{225}Ac-PSMA-617 treatment and 13 of whom were ^{225}Ac-PSMA-617 treatment naïve. Twenty-seven of the patients had extensive skeletal metastases on baseline ^{68}Ga-PSMA-11 PET/CT imaging, and 1 had lymph node–dominant disease and an advanced primary prostatic tumor. Patients were treated with a fixed dose of 100 KBq/kg body weight of ^{225}Ac-PSMA-617 at intervals of 8 wk up to a cumulative dose of 62.9 MBq (range, 25–62.9 MBq; median of 3 cycles; range, 1–7 cycles). In assessments performed at 8 wk after the first cycle and at end-of-treatment follow-up, a >50% decrease in serum prostate-specific antigen was seen in 25% and 39% of participants at the respective time points. Median progression-free and overall survival times were 12 and >17 mo after initial treatment, respectively. PET Response Criteria in Solid Tumors 1 assessment of molecular response could be performed in 22 (78.6%) patients and indicated complete response in 2 (9%), partial response in 10 (45.4%), stable disease in 2 (9%), and progressive disease in 8 (36%) patients. Disease control rates as calculated first from biochemical and then molecular tumor response criteria were 82% and 63.6%, respectively. Multivariate analyses indicated that increasing prostate-specific antigen progression was adversely prognostic for overall survival, whereas any prostate-specific antigen reduction was a positive prognostic indicator of progression-free survival. No grade III/IV toxicities were noted, with the most common reported side effects being transient fatigue (50%) and grade I/II xerostomia (29%). The authors concluded that "^{225}Ac-PSMA-617 targeted α therapy showed promising disease control rates, even when all other therapeutic options were exhausted, with low treatment-related toxicities."

Theranostics

DTC Persistent Disease Tumor Burden and Treatment

Ciappuccini et al. from the François Baclesse Cancer Centre (Caen), Caen University/Caen University Hospital, and Rouen University (all in France) reported on August 13 ahead of print in *BMC Cancer* (2020;20[1]:765) on a study correlating tumor burden of persistent disease in differentiated thyroid cancer with American Thyroid Association (ATA) risk stratification and effect on response to initial therapy and outcomes. The retrospective study included 618 patients with differentiated thyroid cancer referred for ^{131}I treatment. Postoperative data were used to risk stratify patients per the ATA criteria prior to treatment. Posttreatment tumor burden was classified by volume as very small (presence of abnormal foci on postradioiodine scintigraphy with SPECT/CT or ^{18}F-FDG PET/CT without identifiable lesions on anatomic imaging), small (largest legion <10 mm), or large (largest legion ≥10 mm) persistent disease. Persistent disease was seen in 107 patients over a mean follow-up of 7 ± 3 y. Increases in large-volume persistent disease were significantly correlated with ATA-stratified risk, with a significant trend for a decrease in excellent response rate from the very small-, small-, to large-volume groups at 9–12 mo after initial therapy and at last follow-up. Additional analyses indicated that age ≥45 y, distant and/or thyroid bed disease, small- or large-volume tumor burden, and ^{18}F-FDG–positive persistent disease were independent risk factors for indeterminate or incomplete response at last follow-up. The authors summarized their findings that "the tumor burden of persistent disease correlates with the ATA risk

stratification, affects the response to initial therapy, and is an independent predictor of residual disease after a mean 7-y follow-up." They added that this variable may be useful in addition to postoperative ATA risk stratification in refining outcome prognostication after initial treatment.

BMC Cancer

PET/CT vs Bone Scan in Pediatric Sarcoma

In an article e-published on August 18 ahead of print in the *Journal of Pediatric Hematology/Oncology*, Tal et al. from Albert Einstein College of Medicine (New York, NY) and the Montefiore Medical Center (Bronx, NY) compared identification of osseous metastases using bone scanning with that using ^{18}F-FDG PET/CT at diagnosis and relapse in a pediatric sarcoma population. The retrospective study included chart reviews of paired bone scan and PET/CT imaging in 16 patients with osseous sarcoma and 15 with Ewing sarcoma. Fifteen patients had distant osseous metastases. The report also included a review of the pertinent literature. In the patients with osseous sarcoma, 8 of 16 had osseous metastases, with 100% detected on PET/CT and 75% on bone scan. A total of 31 bony lesions were identified on imaging in this patient group: 100% on PET/CT and only 29% on bone scan. Six of the 15 patients with Ewing sarcoma had osseous metastases, with 100% detected on PET/CT and 50% on bone scan. A total of 18 bony lesions were seen on imaging in this patient group: 94% on PET/CT but only 28% on bone scan. The authors concluded that these findings suggest that for pediatric patients with osseous sarcoma or Ewing sarcoma, osseous metastases are more likely to be detected using ^{18}F-FDG PET/CT.

Journal of Pediatric Hematology/Oncology

^{18}F-FDG and ^{18}F-NaF PET in Carotid Atherosclerosis and Stroke

Kim et al. from Chung-Ang University Hospital/Chung-Ang University College of Medicine, Korea University Medical Center/Korea University College of Medicine, and Seoul National University (all in Seoul, Korea) reported in the September issue of the *Journal of Lipid and Atherosclerosis* (2020;8[2]:232-241) on a study looking at tracer uptake patterns in ^{18}F-FDG and ^{18}F-sodium fluoride (^{18}F-NaF) PET in carotid atheroma patients after acute stroke or transient ischemic attacks. The study included 18 patients with ≥50% proximal internal carotid artery stenosis on brain CT angiography, with 36 involved carotid arteries, and 10 patients diagnosed as having experienced acute cerebral infarction. All patients underwent ^{18}F-FDG and ^{18}F-NaF PET imaging after clinical stabilization. Tracer uptakes were compared by target-to-blood ratios according to calcification burden, atheroma volume, and presence or absence of a necrotic core of carotid atheroma. The authors found that ^{18}F-FDG uptake in symptomatic carotid arteries was significantly more increased than that in asymptomatic arteries, whereas ^{18}F-NaF uptake showed no such differentiation. ^{18}F-NaF uptake increases were correlated with calcification burden increases. The authors concluded that "carotid evaluation by ^{18}F-FDG is superior to ^{18}F-NaF PET in the detection of symptomatic carotid atherosclerosis among stroke patients," but that ^{18}F-NaF uptake on PET reflects overall calcification burden.

Journal of Lipid and Atherosclerosis

Molecular Pathology and Neurodegeneration in AD

In an article e-published on August 18 ahead of print in *Cerebral Cortex*, Iaccarino et al. from the University of California San Francisco, the University of California Berkeley, the Lawrence Berkeley National Laboratory (CA), and the VU University Medical Center (Amsterdam, The Netherlands) reported on a study designed to explore the spatial relationships of β-amyloid (Aβ), tau, and neurodegeneration in Alzheimer disease (AD). The study included 81 amyloid-positive patients (median age, 64.4 ± 9.5 y) diagnosed with AD dementia or AD-related mild cognitive impairment who had undergone ^{11}C-PiB, ^{18}F-flortaucipir, and ^{18}F-FDG PET and 3T MR imaging. The study also included 31 amyloid-positive, cognitively normal participants (median age, 77.3 ± 6.5 y). Using comparative data from amyloid-negative cognitively normal adults, neurodegeneration (ND) voxel maps were created for study participants. Aβ-associated pathology showed the greatest proportion of cortical gray matter suprathreshold voxels (spatial extent) for both symptomatic (median, 94%) and asymptomatic participants (median, 55%), followed by tau (79% and 11%, respectively), and ND (41% and 3%, respectively). For both groups, the most frequent hierarchy was amyloid > tau > ND, followed by tau > amyloid > ND and amyloid > ND > tau. For the symptomatic group, most abnormal voxels were ^{11}C-PiB– and ^{18}F-flortaucipir–positive and ND-negative. The majority (91%) of ND-positive voxels were correlated with molecular pathology. Amyloid spatially exceeded tau and ND, with individual heterogeneities. These findings led the authors to conclude that "molecular pathology and neurodegeneration showed a progressive overlap along AD course, indicating shared vulnerabilities or synergistic toxic mechanisms."

Cerebral Cortex

Reviews

Review articles provide an important way to stay up to date on the latest topics and approaches through valuable summaries of pertinent literature. The Newsline editor recommends several general reviews accessioned into the PubMed database in July and August. In an article published on August 6 in the *Journal of Clinical Medicine* (2020;9[8]:E2548) Romanò et al. from the University of Milan (Italy), the National Institute for Infective Diseases "La Spallanzani" (Rome, Italy), AOU Sant'Andrea (Rome, Italy), the IRCCS Istituto Ortopedico Galeazzi (Milan, Italy), Ente Ospedaliero Cantonale (Bellinzona, Switzerland), Lausanne University Hospital/University of Lausanne (Switzerland), the Hospital of the University of Pennsylvania (Philadelphia),

the University of Groningen (The Netherlands), Cliniques Universitaires Saint-Luc (Brussels, Belgium), AZ Groeninge/KU Leuven (Kortrijk, Belgium), "Sapienza" University of Rome (Italy), and the Donald and Barbara Zucker School of Medicine at Hofstra/Northwell (Hempstead, NY) summarized "The role of imaging techniques to define a periprosthetic hip and knee joint infection: Multidisciplinary consensus statement." Raji et al. from the David Geffen School of Medicine at the University of California, Los Angeles and the Mallinckrodt Institute of Radiology at Washington University in St. Louis (MO) offered an overview of "Optimizing use of neuroimaging tools in evaluation of prodromal Alzheimer's disease and related disorders" online ahead of print in the *Journal of Alzheimers Disease.* "Current applications for nuclear medicine imaging in pulmonary disease" were reviewed by Kusmirek et al. from the University of Wisconsin (Madison) on July 22 ahead of print in *Current Pulmonology Reports.* Bauckneht et al. from the IRCCS Ospedale Policlinico San Martino (Genoa), the University of Brescia/Spedali Civili Brescia, IRCSS Regina Elena National Cancer Institute (Rome), the University of Bari Aldo Moro, AO Brotzu (Cagliari), Sapienza University of Rome, the University of Messina, the University of Padova, and the Fondazione Istituto G. Giglio (Cefalù; all in Italy) published on August 16 in *Diagnostics (Basel)* (2020;10[8]:E598) on "Somatostatin receptor PET/CT imaging for the detection and staging of pancreatic NET: A systematic review and meta-analysis." In an overview released online on July 27 ahead of print in *Current Medical Chemistry*, Mengshu and colleagues from the University of Iowa (Iowa City), Viewpoint Molecular Targeting, Inc. (Coralville, IA), Eichrom Technologies, LLC (Lisle, IL), Lantheus Medical Imaging (Billerica, MA), the U.S. Department of Energy (Oak Ridge, TN), the National Institute of Standards and Technology (Gaithersburg, MD), and Sciencons AS (Oslo, Norway) looked at "$^{203/212}$Pb theranostic radiopharmaceuticals for image-guided radionuclide therapy for cancer." Fur et al. from the Massachusetts General Hospital/Harvard Medical College (Boston) published "Toward molecular imaging of intestinal pathology" on August 14 online ahead of print in *Inflammatory Bowel Diseases.*